

COMPARISON OF THE NOISE POWER SPECTRUM PROPERTIES OF  
MEDICAL X-RAY IMAGING SYSTEMS

ZEKI AHMED DARWISH

A thesis submitted in fulfillment of the  
requirements for the award of the degree of  
Master of Science (Physics)

Faculty of Science  
Universiti Teknologi Malaysia

FEBRUARY 2011

To His Highness Sheikh Hamdan bin Zayed Al Nahyan

## ACKNOWLEDGEMENT

I would like to express my gratitude and heartfelt thanks to my supervisor Assoc. Prof. Dr Wan Muhamad Saridan Wan Hassan for his supervision, guidance, advice and support that has enabled me to develop an understanding of the subject. He has helped a great deal with advice concerning language correction and programming shortcuts and has helped to put many problems in perspective. I am indebted to him more than he knows.

I wish to gratefully acknowledge Dr. C. Koedooder at the Academic Medical Center, Radiotherapy Department. Amsterdam, Netherland, for sending me his thesis along with many articles that were difficult to get at the beginning of my research, and for encouraging me to complete my studies. Special thanks to my former professors at the University of Basrah-Iraq, Dr. Dia Ahmed Al-Mukhtar, Dr. Mansoor Muhamad and Dr. Hashim A. Qassem. I would also like to thank my uncle Mr. Dumad. J. Ali, who stimulated my interest in learning, and my best friends, Dr Amer.Al Nasrri, Dr Abbass Hashim, Dr Shubair.A, Dr. Sabah Mahdi, Rasel.S and Marrof. Al Rifai, whose assistance was perpetually refreshing, helpful and memorable, finally, I would like to acknowledge my colleagues at Wadi Al- Hillo School in U.A.E in particular Mr. Jamal Al-Zubaidi, Mr. Abdullah Qumber school director and his assistant Mr.Saif Bin Khamis for their continuous encouragement to me in completing this study.

Words fail me to express my appreciation to my wife and my sisters whose dedication, love and persistent confidence in me have taken the load off my shoulders. A big hug to my beloved daughter Al Zahraa; you are the sunshine of my live. To my father and mother, who have passed away, I apologize to you; I cannot find the words to say. You have achieved this dream, but it came too late.

## ABSTRACT

Noise in medical images is recognized as an important factor that determines the image quality. Image noise is characterized by noise power spectrum (NPS). Four methods of NPS determination were compared: Wagner, Beutel, Dobbins and Samei's methods on Lanex Regular/ TMG screen-film system and Hologic Lorad Selenia Full Field Digital Mammography system, with the aim of selecting the best method to use. These methods differ in terms of various parametric choices and algorithm implementations. The one-dimensional moving-slit method has been used in the past to characterize the NPS of analogue screen film system (Wagner's method). Beutel's method offers the advantage of providing a value of the NPS at zero frequency along with NPS calculated via autocorrelation function (ACF). The moving slit and ACF methods have been replaced by a 2-D Fourier analysis method with the advent of fast Fourier transform and faster computers. This method is based on two techniques. The first is based on the extraction of a one-dimensional slice through the two-dimensional NPS parallel to and immediately adjacent to the axes (Dobbins's method). The second is based on the extraction of a one-dimensional slice through the two-dimensional NPS, just on the axes (Samei's method). NPS computation using different methods have been attempted using codes written in MATLAB. Overall, the four methods generate a practical value of noise power spectrum between  $10^{-3} - 10^{-6} \text{ mm}^2$  at spatial frequency range  $0 - 10 \text{ mm}^{-1}$ . It was found that the Dobbins's method was the best method for NPS determination.

## ABSTRAK

Hingar dalam imej perubatan dikenalpasti sebagai faktor penting yang menentukan kualiti imej. Hingar imej dicirikan oleh spektrum kuasa hingar (NPS). Empat kaedah bagi menentukan NPS telah dibandingkan iaitu kaedah Wagner, Beutel, Dobbins dan Samei ke atas sistem skrin-filem Lanex Regular/ TMG dan sistem mamografi digital medan penuh Hologic Selenium Lorad, dengan tujuan untuk memilih kaedah terbaik untuk digunakan. Kaedah-kaedah yang digunakan adalah berbeza dari segi pilihan pelbagai parameter dan implementasi algoritma. Kaedah celah bergerak satu dimensi telah digunakan sebelum ini bagi mencirikan NPS sistem skrin filem analog (kaedah Wagner). Kaedah Beutel mempunyai kelebihan dari segi memberikan nilai NPS pada frekuensi sifar dan mengira NPS melalui fungsi autokorelasi (ACF). Kaedah celah bergerak dan kaedah ACF telah digantikan oleh kaedah analisis Fourier 2-D dengan terciptanya transformasi Fourier cepat dan komputer yang lebih laju. Kaedah ini berdasarkan dua teknik. Yang pertama berdasarkan pemilihan hirisan satu dimensi melalui NPS dua dimensi selari dan bersebelahan paksi (kaedah Dobbins). Yang kedua berdasarkan pemilihan hirisan satu-dimensi melalui NPS dua-dimensi, hanya pada paksinya (kaedah Samei). Pengiraan NPS menggunakan kaedah-kaedah yang berbeza telah dilakukan dengan menggunakan kod yang ditulis dalam MATLAB. Secara keseluruhan empat kaedah itu menjana nilai praktikal spektrum kuasa hingar antara  $10^{-3} - 10^{-6} \text{ mm}^2$  pada julat frekuensi ruang  $0 - 10 \text{ mm}^{-1}$ . Telah didapati bahawa kaedah Dobbins adalah kaedah yang terbaik untuk penentuan NPS.

## TABLE OF CONTENTS

CHAPTER	TITLE	PAGE
	<b>DECLARATION</b>	<b>ii</b>
	<b>DEDICATION</b>	<b>iii</b>
	<b>ACKNOWLEDGEMENT</b>	<b>iv</b>
	<b>ABSTRACT</b>	<b>v</b>
	<b>ABSTRAK</b>	<b>vi</b>
	<b>TABLE OF CONTENTS</b>	<b>vii</b>
	<b>LIST OF TABLES</b>	<b>xi</b>
	<b>LIST OF FIGURES</b>	<b>xii</b>
	<b>LIST OF SYMBOLS</b>	<b>xviii</b>
	<b>LIST OF ABBREVIATIONS</b>	<b>xix</b>
	<b>LIST OF APPENDICES</b>	<b>xxi</b>
<b>1</b>	<b>INTRODUCTION</b>	<b>1</b>
	1.1 Background of Study	1
	1.1.1 Screen Film System	5
	1.1.2 Digital Detector Technology	6
	1.2 Problem Statement	8
	1.3 Objectives of Study	9
	1.4 Scope of Study	9
	1.5 Aim of Study	10
	1.6 Significance of Study	10
	1.7 Images Used in Study	10

1.8	Outline of Thesis	11
<b>2</b>	<b>LITERATURE REVIEW &amp; THEROY</b>	<b>12</b>
2.1	Fast Fourier Transform	12
2.2	Noise Analysis	13
2.2.1	Wiener Spectrum Calculation	18
2.2.1.1	Electronic Filtering	18
2.2.2	Direct and Indirect Methods of WS Calculation	18
2.2.2.1	Fourier Transform of Autocorrelation Function	19
2.2.2.2	Fast Fourier Transform Digital Method	20
2.2.2.3	Direct Method for Measurement of NPS	21
<b>3</b>	<b>METHODOLOGY</b>	<b>24</b>
3.1	Introducation	24
3.2	Image Preparation	26
3.3	Computer Programs	27
3.4	NPS Computation Methods	29
3.4.1	Wagner's Method	29
3.4.2	Beutel's Method (Autocorrelation)	32
3.4.3	Dobbin's Method	33
3.4.4	Samei's Method	35
<b>4</b>	<b>RESULTS AND DISCUSSION</b>	<b>42</b>
4.1	Introduction	42
4.2	Wagner Method	42
4.2.1	Low Pass Filter	42
4.2.2	Low Frequency Filtering	44
4.2.3	Slit Length	46

4.2.4	Length of Fast Fourier Transform	48
4.2.5	Overlapping and Nonoverlapping Blocks	49
4.2.6	Welch Window	51
4.2.7	Normalization	54
4.2.8	Smoothing	56
4.2.9	Aperture Correction	57
4.2.10	Summary of Wagner's Method	58
4.3	Beutel's Method	59
4.3.1	Low Pass Filter	59
4.3.2	Effect of Pixel Size	60
4.3.3	Length of Fast Fourier Transform	61
4.3.4	Data Shifting Factor K	62
4.3.5	Normalization	66
4.3.6	Summary of Beutel's Method	67
4.4	Dobbins's Method	68
4.4.1	Slice from the 2D NPS	68
4.4.1.1	One Slice Adjacent to Axis	68
4.4.1.2	Two Slices Adjacent to Axis	70
4.4.1.3	Four Slices Adjacent to Axis	73
4.4.1.4	Eight Slices Upper $u$ -Axis	75
4.4.1.5	Eight Adjacent Slices	77
4.4.1.6	Comparison of NPS Estimates from Different Slices	79
4.4.2	The Effect of Pixel Size on NPS Measurement	81
4.4.3	Fourier Length and NPS Estimates	83
4.4.4	Normalized Noise Power Spectrum (NNPS)	84
4.4.5	A radial Symmetric NNPS	87
4.4.6	Overlapping and Nonoverlapping ROI	88
4.4.7	Size of ROI	90
4.4.8	Summary of Dobbin's Methods	97
4.5	Samei's Method	97
4.5.1	One Line of Center Axis	98
4.5.2	Five Lines on Center Axis	99
4.5.3	Ten Lines on Axis	101

4.5.4	Comparison Measurements NPS from Different Lines	102
4.5.5	Windowing	104
4.5.6	Normalized NPS	106
4.5.7	Overlapping and Nonoverlapping ROI	109
4.5.8	Pixel Size	111
4.5.9	Size of ROI	113
4.5.10	Summary of Samei's Method	118
4.6	Comparison of Methods	119
<b>5</b>	<b>SUMMARY AND CONCLUSION</b>	<b>124</b>
5.1	Summary of the Research	124
5.2	Contribution of Study	126
5.3	Conclusion	126
5.4	Future Directions	130
5.5	Closing Remarks	131
	<b>REFERENCES</b>	<b>132</b>
	<b>Appendices A - I</b>	<b>143 - 182</b>

## LIST OF TABLES

TABLE NO.	TITLE	PAGE
3.1	Detailed information on the images used in this research	26
4.1	Details of curves in Figure 4.1	43
4.2	Detailed information on the number of running average points related to Figure 4.2	44
4.3	Details of curves in Figure 4.4	46
4.4	Detailed comparison of length of FFT related to Figure 4.6	48
4.5	Details of the NPS for curves in Figs(4.9 and 4.10)	50
4.6	Comparison of the area under WS curves for each of different normalizations	55
4.7	Details for the NPS curves, with filter and without filter in Figure 4.17	59
4.8	Details for the NPS curves related to Figure 4.18	61
4.9	Effect of fast Fourier transform length in the NPS curves in Figure 4.19	62
4.10	Testing ( $k$ ) factor used several different images	63
4.11	Values of the area under the curves related to Figure 4.28	69
4.12	Details of NPS curves obtained from eight Slices upper $u$ -axis	76
4.13	Comparison among the ROI sizes for different factors	91
4.14	Details of area and volume related to Figure 4.77, Figure 4.78 and Figure 4.79	107
4.15	Comparison among the ROI sizes for different factors	113
4.16	Parameters for the NPS methods	120

## LIST OF FIGURES

FIGURE NO.	TITLE	PAGE
1.1	Image quality triangle: illustrates the Wiener spectrum in relation to parameters and physical image measurements adapted from Marsh and Malone (2001)	3
1.2	A conventional screen film radiographic receptor	5
1.3	A characteristic curve of a film that gives the relationship between optical density and relative exposure	6
1.4	Schematic picture of amorphous detector adapted from Granfors and Aufrichtig (2000)	7
1.5	A picture illustrating characteristic curve of mammography film to show that the display contrast (slope of curve) is suboptimal in lucent and dense regions of the breast adapted from smith (2003)	8
1.6	Images used in the study	11
3.1	The flow chart of the research methodology	25
3.2	The fluctuation in image pixel value (1000x1000) pixels	27
3.3	The fluctuation in image pixel value in one row of the image	27
3.4	Calibration of optical density and pixel brightness	28
3.5	Low pass filter	29
3.6	Selection of the ROI from image	34
3.7	Slice from 2-D NPS parallel to primary axis of interest, the white dotted lines represents vertical NPS. The white lines represent horizontal NPS	35
3.8	Slices used to generate horizontal and vertical 1-D NPS	37
3.9	Block diagram describing steps to calculate NPS by Wagner's method	38
3.10	Block diagram describing steps to compute the NPS by Beutel's	

	method	39
3.11	Block diagram describing steps to compute the NPS by Dobbins's method	40
3.12	Block diagram describing steps to calculate the NPS by Samei's method	41
4.1	Effect of low pass filter for different cases	43
4.2	Low frequency filtering with different number of running average points	45
4.3	The effect of low frequency filtering for different cases	45
4.4	The effect of varying the synthesized slit length of scanning aperture on the NPS using Image A1.bmp	47
4.5	Plot of NPS against synthesized slit length for selected spatial frequencies	47
4.6	NPS values for different values of FFT length using Image A1.bmp	48
4.7	Image divided into distinct blocks	49
4.8	Image divided into distinct blocks with specified overlaps	49
4.9	Comparison of the NPS values for overlapping and non- overlapping blocks, $L=32$	50
4.10	Comparison of the NPS values for overlapping and non-overlapping blocks, $L=256$	51
4.11	Welch window commonly used in NPS estimation with Wagner method	52
4.12a	Effect of Welch window on the NPS, linear- linear plot	53
4.12b	Effect of Welch window on the NPS, Semilog plot	53
4.13	The Wiener spectrum normalised by different factors	55
4.14	Correction factor for smoothing of density fluctuation data	56
4.15	Comparison between two smoothings	57
4.16	Comparison of the NPS values for aperture correction and without aperture correction	58
4.17	NPS values were measured with low pass filter and without filter	60
4.18	NPS values for 128x128 ROI at 0.0100, 0.0125, 0.0150 mm pixel size	61
4.19	Comparison of NPS curves with different values of the	

	length of Fourier transform	62
4.20	Comparison of NPS values of two versions of factor ( $k$ ) using Image A1.bmp	63
4.21	Comparison of NPS values of two versions of factor ( $k$ ) using Image A3.bmp	64
4.22	Comparison of NPS values of two versions of factor ( $k$ ) using Image file 0000.bmp	64
4.23	Comparison of NPS values of two versions of factor ( $k$ ) using Image file 0001.bmp	65
4.24	Comparison of NPS values for factor ( $i+k$ ) among different images	65
4.25	Comparison of NPS values for factor ( $j+k$ ) among different images	66
4.26	Normalisation of the NPS via ACF	67
4.27	Slices used to generate horizontal and vertical 1-D NPS	69
4.28	2-D NPS, horizontal and vertical 1-D NPS estimates from one slice adjacent to axis	70
4.29	Two rows (1,2) and columns (1',2') were used to generate horizontal and vertical 1-D NPS	71
4.30	NPS values, 2-D NPS, 1-D vertical and horizontal for two slices adjacent to axis	71
4.31	Comparison between 2-D NPS values for two slices left and two slices right of $v$ -axis	72
4.32	Comparison between horizontal 1-D NPS values for two slices upper $u$ -axis in left and right side	72
4.33	Comparison between vertical 1-D NPS values for two slices adjacent to $v$ -axis in left and right side	73
4.34	Slices used to generate horizontal and vertical 1-D NPS	74
4.35	NPS values, 2-D, 1-D vertical and horizontal for four slices adjacent to $u$ -axis and four slices adjacent to $v$ -axis	74
4.36	Rows and columns data used to generate horizontal and vertical 1-D NPS	75
4.37	NPS values, 2-D and 1-D vertical and horizontal for eight slices upper $u$ - axis	76
4.38	Eight slices used to generate vertical and horizontal 1-D NPS in two different cases	77

4.39	Comparison between 1-D NPS of eight horizontal slices in two different cases	78
4.40	Comparison between 1-D NPS of eight vertical slices in two different cases	78
4.41	Comparison between 2-D NPS for eight slices in two different cases	79
4.42	1-D NPS (horizontal) values for the different slices	80
4.43	1-D NPS (vertical) values for the different slices	80
4.44	2-D NPS values for the different slices	81
4.45	2-D NPS measured at 0.0100 mm, 0.0125 mm and 0.0150 mm pixel size	82
4.46	NPS- vertical measured at 0.0100 mm, 0.0125 mm and 0.0150 mm pixel size	82
4.47	NPS- horizontal measured at 0.0100mm, 0.0125mm and 0.0150mm pixel size	83
4.48	NPS values are shown for the different length of FFT	84
4.49	Normalized 2-D NPS taken from four slices adjacent to $u$ and $v$ - axis	85
4.50	Normalized 1-D NPS horizontal taken from four slices adjacent to $u$ -axis	86
4.51	Normalized 1-D NPS vertical taken from four slices adjacent to $v$ -axis	86
4.52a	A radial symmetric NPS values, 2-D and 1-D horizontal and vertical	87
4.52b	Total 2-D NPS taken from Image A3.bmp	88
4.53	NPS values for 64x64 size of overlapping and non-overlapping ROI	89
4.54	NPS values for 128x128 size of overlapping and non-overlapping ROI	89
4.55	NPS values for 256x256 size of overlapping and non-overlapping ROI	90
4.56	Choice of ROI from original Image A3.bmp	91
4.57	1-D NPS horizontal, vertical and 2-D NPS values for 32x32 ROI size	92

4.58	Meshz-plot 2-D NPS for 32x32 ROI size	92
4.59	Two-dimensional NPS plotted vs. $u$ and $v$ -spatial frequency for 64x64 ROI size	93
4.60	Meshz -plot 2-D NPS for 64x64 ROI size	93
4.61	Two-dimensional NPS plotted vs. $u$ and $v$ -spatial frequency for 128x128 ROI size	94
4.62	Meshz -plot 2-D NPS for 128x128 ROI size	94
4.63	1-D NPS horizontal, vertical and 2-D NPS(R) values for 256x256 ROI size	95
4.64	Meshz -plot 2-D NPS for 256x256 ROI size	96
4.65	Comparison of the NPS values for various ROI sizes	96
4.66	One row and column on the center axis used to generate horizontal and vertical 1-D NPS	98
4.67	2-D NPS and NPS directional dependence were obtained from one row and column on the center axis	99
4.68	Lines used to generate the NPS directional dependence	100
4.69	2-D NPS and directional dependence for 5 lines on the central axis	100
4.70	Lines used to generate 1-D NPS horizontal and vertical	101
4.71	2-D NPS and directional dependence for 10 lines on the central axis	102
4.72	Comparison of the NPS values for various vertical lines	103
4.73	Comparison of the NPS values for various horizontal lines	103
4.74	Comparison of the 2- NPS values for various lines	104
4.75	Hamming window commonly used in NPS estimation in Samei's method	105
4.76	Effect of Hamming window on measurement of the NPS	106
4.77	Normalized 2-D NPS measured from 20 lines on the central axes	107
4.78	Normalized 1-D NPS horizontal measured from 10 lines on the $v$ -axis	108
4.79	Normalized 1-D NPS vertical measured from 10 lines on the $u$ -axis	108
4.80	NPS values for the overlapping and non-overlapping for 64x64 ROI size	109

4.81	NPS values for the overlapping and non-overlapping for 128x128 ROI size	110
4.82	NPS values for the overlapping and non-overlapping for 256x256 ROI size	110
4.83	Comparison of the 2-D NPS values at 0.0100 mm, 0.0125 mm and 0.0150 mm pixel size	111
4.84	Comparison the 1-D NPS values in the vertical direction at 0.0100 mm, 0.0125 mm and 0.0150 mm pixel size	112
4.85	Comparison of the 1-D NPS values in the horizontal direction at 0.0100 mm, 0.0125 mm and 0.0150 mm pixel size	112
4.86	1-D NPS horizontal, vertical and 2-D NPS values for 32x32 ROI	114
4.87	Meshz-plot 2-D NPS for 32x32 ROI	114
4.88	1-D NPS horizontal, vertical and 2-D NPS values for 64x64 ROI	115
4.89	Meshz-plot 2-D NPS for 64x64 ROI	115
4.90	1-D NPS horizontal, vertical and 2-D NPS values for 128x128 ROI	116
4.91	Meshz-plot 2-D NPS for 128x128 ROI size	116
4.92	1-D NPS horizontal, vertical and 2-D NPS values for 256x256 ROI	117
4.93	Meshz-plot 2-D NPS for 256x256 ROI size	117
4.94	Comparison of the NPS values for various ROI sizes	118
4.95	Comparison of the NPS values for, Wagner, Beutel, Dobbins and Samei methods using Image A1.bmp	123
4.96	Comparison of the NPS values for, Wagner, Beutel, Dobbins and Samei methods using Image file0000.bmp	123

## LIST OF SYMBOLS

$W_T(u)$	-	System radiographic noise
$W_Q(u)$	-	Quantum mottle
$W_G(u)$	-	Film graininess
$W_S(u)$	-	Screen structure mottle
$D_t$	-	Gross optical density
$D_g$	-	Optical density of a film associated with developed silver halide grains
$D_b$	-	Optical density of the film base
$\bar{D}$	-	Average optical density
$c(x, y)$	-	Autocorrelation function
CsI	-	Cesium iodide
a-Se	-	Amorphous selenium
$h(x, y)$	-	Point spread function
$(x, y)$	-	Spatial coordinates
$(u, v)$	-	Spatial frequency coordinate
$u_N$	-	Nyquist frequency
$\Delta u, \Delta v$	-	Spatial frequency resolution
$W_i$	-	Welch window
$H(r)$	-	Hamming window

**LIST OF ABBREVIATIONS**

WS	-	Wiener spectrum
NPS	-	Noise power spectrum
NNPS	-	Normalized noise power spectrum
LP	-	Line- pairs in a space of one millimeter
SNR	-	Signal-to-noise ratio
MTF	-	Modulation transfer function
CCD	-	Charge-coupled device
SF	-	Screen film
ACF	-	Autocorrelation function
ACVF	-	Autocovariance function
TFT	-	Thin film transistor
AAPM	-	American Association of Physicists in Medicine
IEC	-	International Electrotechnical Commission
DR	-	Digital radiography
CR	-	Computed radiography
NEQ	-	Noise equivalent quanta
DQE	-	Detective quantum efficiency
FFDM	-	Full field digital mammography
FFT	-	Fast Fourier transforms

ROI	-	Region of interest
ADC	-	Analog-to-digital converter
LR/TMG	-	Lanex Regular /T Mat G

**LIST OF APPENDICES**

<b>APPENDIX</b>	<b>TITLE</b>	<b>PAGE</b>
A	Programme for Wagner's method	143
B	Programme for Beutel's method	147
C	Programme for Dobbin's method	150
D	Programme for Samei's method	155
E	Numerical results for Wagner's method	161
F	Numerical results for Beutel's method	169
G	Numerical results for Dobbin's method	176
H	Numerical results for Samei's method	179
I	Publications	182

# CHAPTER 1

## INTRODUCTION

### 1.1 Background of Study

Noise is often defined as uncertainty in signal due to random fluctuations in that signal. There are many causes for these fluctuations. For example, an X-ray beam emerging from an X-ray tube inherently is statistical in nature. That is, the number of photons emitted from the source per unit time varies according to a Poisson distribution. The Wiener spectrum (WS) represents the noise power spectrum in an image as a function of spatial frequency. It, therefore, represents the relationship between noise and spatial resolution (Dobbins III, 2000).

WS provides the means of characterizing image noise and plays a central role in ultimate measure of image quality. The noise in images is recognized as an important factor in determining image quality. Image noise may be characterized by the WS or noise power spectrum (NPS) (Hanson, 1998).

The NPS may be understood in several but equivalent ways. It may be thought of as the variance of image intensity (i.e., image noise) distributed among various frequency components of the image; or may be pictured as the variance of a given spatial frequency component in an ensemble of measurements in that spatial frequency (Marsh and Malone, 2001).

The medical image is a window into the human body; it is formed by the imaging modalities that use various forms of radiation and energy to open the body

to visualization from the interactions of energy with human tissue. The main interactions of the X-ray and tissue are in the forms of photo- electric effect and Compton scattering. Images formed by screen film imaging systems consist of a two dimensional optical density pattern on a photographic film. The process by which the density pattern is formed (often called the imaging chain) can be thought of as a serial sequence of three operations (Metz and Doi, 1979). (1) Passage of a beam of X-ray through the object to generate a two dimensional pattern of X-ray intensity which is incident on the recording system (screen film system); (2) interaction of the X-ray intensity pattern with screen phosphor to convert the X-ray intensity pattern into a light intensity pattern which is incident on photographic film; and (3) interaction of the light intensity pattern with the photographic emulsion to produce a latent image which after development yields a pattern.

Image quality is determined by a combination of five more specific image characteristics. They are: (1) Contrast (2) Blurring (3) Artifacts (4) Spatial (geometric) characteristics (5) Visual noise. Contrast is the variation in film density (shades of gray) that actually forms the image or may be defined as a measure of relative brightness difference between two locations in an image (Cunningham 2000). Without contrast there is no image. The film contrast between two areas is expressed as the difference between the density values. Blurring reduces a characteristic that is known as spatial resolution. Resolution is expressed in terms of the number of line-pairs in a space of one mm that are visible. Increasing LP/mm generally relates to increasing detail. Therefore, a high spatial resolution indicates high (good) visibility of anatomical detail. Spatial characteristics are related to geometric unsharpness such as focal spot size and object magnification. Spatial resolution also refers to the ability of a system to represent distinct anatomic features within the object being imaged (Samei, 2003).

Noise is undesirable image characteristics that reduce the visibility of specific objects. Any component of the signal that does not convey relevant information can be considered as noise (Holland, 1979). Examples of noise are the fluctuations in the source signal, randomness in the detector output, and superimposed structures which are not related to the signal of interest.

In general, image quality is determined by three primary physical parameters: contrast, spatial resolution and noise (Jessen, 2004). These quality parameters can be evaluated by objective image quality measurements such as signal-to-noise ratio (SNR), modulation transfer function (MTF) and Wiener spectra (WS). Together they form a basis for the description of image quality, which encompasses the three primary physical image quality parameters, Figure 1.1.

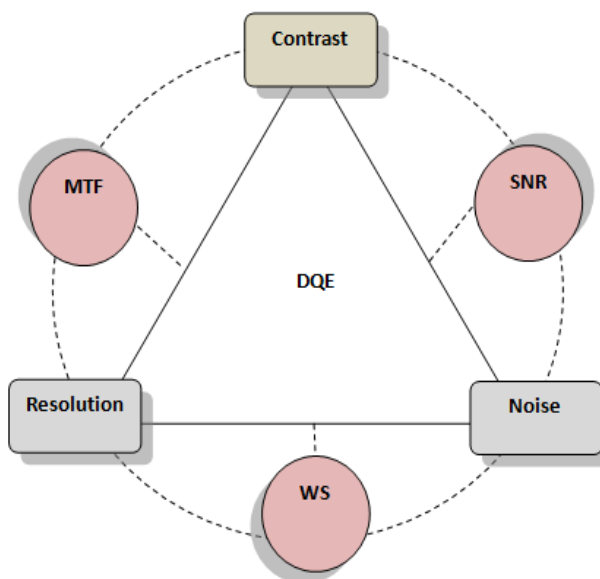


**Figure 1.1** Image quality triangle: illustrates the Wiener spectrum in relation to parameters and physical image measurements. Adapted from Marsh and Malone (2001).

With any imaging system, images are partially degraded by various sources of statistical fluctuation which arise along the imaging chain (Lissak *et al*, 1984). For example, quantum and electronic noise that produces random variations of signal that can obscure useful information in a diagnostic image. Random noise means fluctuations of the signal over an image, as a result of uniform exposure, and can be characterized by the standard deviation of the signal variations over the image of a uniform object. The Wiener spectrum must be used to get a more complete description of the spatial correlation of noise: it measures noise power as a function of spatial frequency (Dobbins *et al*, 2006).

The noise power spectrum (NPS) of a radiographic film can be expressed in three constituent noise sources and can be written as

$$W_T(u) = W_Q(u) + W_G(u) + W_S(u) \quad 1.1$$

where  $W_T$ ,  $W_Q$ ,  $W_G$  and  $W_S$  stand for WS of the system radiographic noise, quantum mottle, film graininess and screen structure mottle respectively, and  $u$  is spatial frequency. Radiographic mottle is the fluctuations of film density from one area to another due to imaging system noise (Rossman, 1963; Doi *et al*, 1982; Wan, 1998).

The primary noise components vary spatially in the number of X-ray quanta absorbed in the screens associated with random structural inhomogeneities in the phosphor coating. Film granularity is a component of radiographic mottle, which is due to the random distribution of developed grains in the processed emulsion. The optical density of a film associated with developed silver halide grains  $D_g$  is given by

$$D_g = D - D_b \quad 1.2$$

where  $D$ ,  $D_b$  are the gross optical density of the film and the optical density of the film base, respectively. Structure mottle is due to fluctuation in the number of X-rays absorbed from one area of the phosphor layers to another arising from random inhomogeneities (as opposed to gross nonuniformities) in the phosphor coating (Barnes, 1982).

Equation 1.1 can be expressed in digital mammography detectors as

$$W_T(u) = W_Q(u) + W_{SQ}(u) + W_D(u) \quad 1.3$$

This equation gives the total (NPS) expressed in terms of electrons generated in image display, where  $W_Q$  is due to the number of X-rays interacting in the screen and the difference in the number of light quanta emitted from the screen per X-rays interaction.  $W_{SQ}$  is due to the statistical fluctuation in the number of secondary quanta

that would occur in the absence of X-ray quantum noise.  $W_D$  is due to inherent detectors output–signal fluctuation caused by the number generation electrons in the CCD readout process (Madiant and Yaffe, 1994). In modern X-ray systems, electronic devices introduce another type of noise (electronic noise) in the system (Zhang *et al*, 2007), (Lazzari *et al*, 2007).

### 1.1.1 Screen Film System

In conventional radiography, a patient is positioned between an X-ray source and the receptor. In screen film radiography, the receptor consists of the film mounted in contact with either one or two intensifying screens, as shown in Figure 1.2.

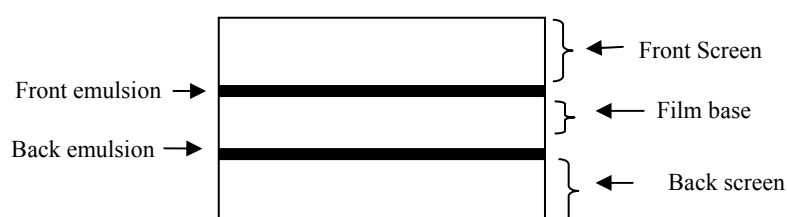


**Figure 1.2** A conventional screen film radiographic receptor.

The cassette contains an intensifying screen which, when exposed to X radiation, converts the radiation to light which exposes a photographic emulsion. The photographic film can be developed to provide an image to the observer. Films with emulsion on both sides of support were first demonstrated by Levy in 1897. For exposure, these were sandwiched between two intensifying screens. The penetrating power of X-ray made it possible to produce similar images on two sides of the film (Van Metter and Dickerson, 1994).

The light of an intensifying screen can, under certain conditions, penetrate the film emulsion and film base to expose the emulsion on the other side of the film base. This is called the crossover effect and causes unsharpness. The light that travels further to the emulsion on the other side is more scattered (Metz and Doi, 1979; Hertrich, 2005).

The relationship between film density and exposure is often presented in the form of a graph, as shown in Figure 1.3. This graph shows the relationship between density and relative exposure. This type of graph is known as either a film characteristic curve or an H & D (Hurter and Driffield) curve (ICRU, 1995).

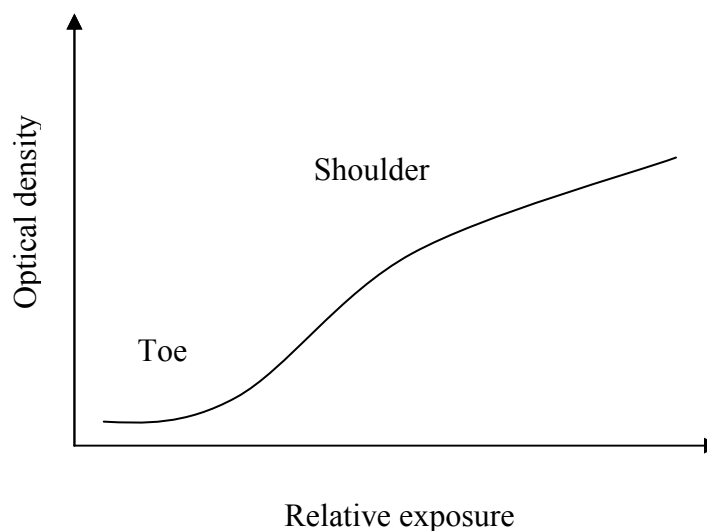


**Figure 1.3** A characteristic curve of a film that gives the relationship between optical density and relative exposure.

### 1.1.2 Digital Detector Technology

A digital X-ray detector is the key component of a digital radiography system. It has to fulfill several requirements concerning field size, pixel size, sensitivity, dynamic range, internal noise and readout. Digital X-ray detector technologies provide several advantages when compared with screen-film (SF) systems: better diagnostic quality of radiographic image, increased dose efficiency, better dynamic range and possible reduction of radiation exposure to the patient. A basic difference between digital detectors and screen film (SF) is that the detection of X-rays and the image display are separated in a digital imaging system. Therefore, the detector can be optimized for detection X-rays. Now the applications of detectors are becoming commercially available. They share the advantage of all digital detectors in that they produce images in digital form. This eliminates the need for a physical film to view

the image and allows images to be stored and transmitted digitally to wherever they need to be viewed (Granfors and Aufrichtig, 2000). Other advantages, of digital detectors are the ability to enhance the images and to analyze the images by computer to improve diagnostic efficiency.

There are two methods of image capture used in digital mammography, which represent different generations of technology: indirect conversion and direct conversion. Direct flat detector systems convert the X-rays directly into electric charge via a layer of material sensitive to radiation (e.g. amorphous selenium, a-Se). In indirect flat detector systems, X-rays first generate visible light in a scintillator (e.g. cesium iodide, CsI, like the image intensifier). Light sensitive photodiodes then convert light into electric charges (Samei, 2003; Hertich, 2005). Figure 1.4 is an example of a digital detector.

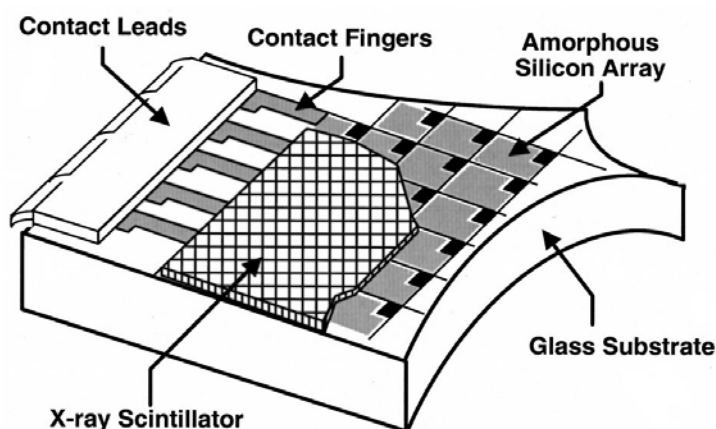


**Figure 1.4** Schematic picture of amorphous detector adapted from Granfors and Aufrichtig (2000).

In direct-conversion digital detectors, spatial resolution is limited only by the size of the pixel. The size of the pixel in these detectors can be made arbitrarily small to make the resolution performance extend to very high spatial frequencies. The ultimate limit of a very small pixel is the reduced X-ray flux impinging upon the detector the pixel size of full field digital mammography (FFDM) system range from 50 to 100 microns (Smith, 2003). The pixel size for the Hologic's selenium is 70 microns and because of the design of this detector, this represents its true resolution characteristic. The maximum spatial resolution of an image is defined by pixel size

and spacing (i.e. the distance between centers of pixels). Digital detectors that have higher sensitivity allow better image quality at all frequencies, showing the ability to represent both small and large image structure as in Figure 1.5.

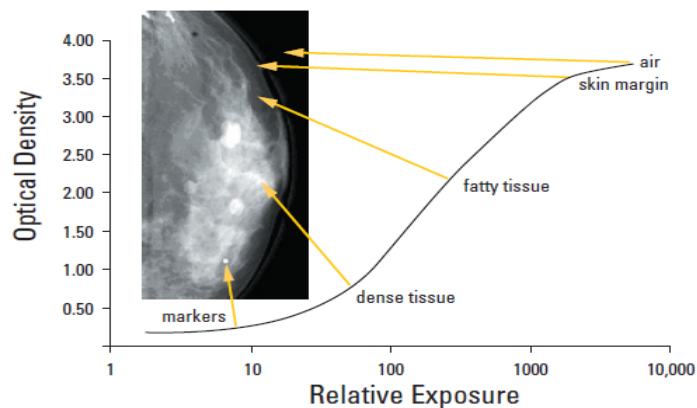


**Figure 1.5** A picture illustrating characteristic curve of mammography film to show that the display contrast (slope of curve) is suboptimal in lucent and dense regions of the breast. Adapted from Smith (2003).

Mammographic imaging requires the detection and classification of extremely small objects. In particular, micro calcifications can be as small as 100 to 200 microns. A useful Full Field Mammographic (FFDM) system must be able to image the smallest micro calcifications.

## 1.2 Problem Statement

The Wiener spectrum is an important tool used to evaluate the noise power spectrum (NPS) of an image in the spatial frequency domain. Many workers have reported on the measurement in the literature. There has been little comparative work done on the relative performance of different imaging modalities using the NPS. The measurement of the WS is not conceptually complicated but difficult to carry out experimentally and there has not been complete agreement on the best methods for these measurements. While there is a considerable literature on NPS computation, in practice the best methodology is not clear. The measurement of the NPS remains a complex subject; in spite of the laudable effort to reach a consensus on the best

measurement methodology, there is still a sizable amount of literature dealing with measurements made on various imaging modalities using a variety of techniques.

### **1.3 Objective of Study**

The main objectives of this study are as follows:

1. To study and analyze different techniques used to evaluate the NPS effect of medical imaging namely
  - Wagner's method
  - Beutel's method
  - Dobbins's method
  - Samei's method
2. To look for the most successful method and program to compute the NPS

### **1.4 Scope of Study**

The scope of the study includes the following steps

1. Collection of images from different sources, and different techniques and systems. Using MATLAB<sup>®</sup> Version 7.8.0.347 (R2009 a), to write special programs to calculate the NPS in four methods mentioned in Section 1.3.
2. Comparison of results, analysis and evaluation to determine the best method to calculate the NPS

3. The focus of study is a comparison of different methods and not different imaging devices.

### **1.5 Aim of Study**

The main purpose of this study is to produce characteristic evidences of the best method of noise analysis associated with X-ray images. The advantages, disadvantages and the consolidation of this method are to be investigated.

### **1.6 Significance of Study**

Noise power spectrum (NPS) is an important concept that has been widely accepted for quantitative evaluation of image quality both in clinical practice and in research. NPS measurements', using both analog and digital systems has been studied in this research. This work will investigate some practical approaches in NPS measurement to using the limited amount of image data acquired to obtain accurate NPS estimations with best frequency resolutions.

### **1.7 Images Used in Study**

This study was conducted at the University Technology Malaysia Skudai, Johor. Figure 1.6 shows images used in the study. Images A1.bmp and A3.bmp were prepared at the Aberdeen Royal Infirmary, Scotland. Images file0000.bmp, file0001.bmp and file0002.bmp were prepared at Putrajaya Hospital, Malaysia.

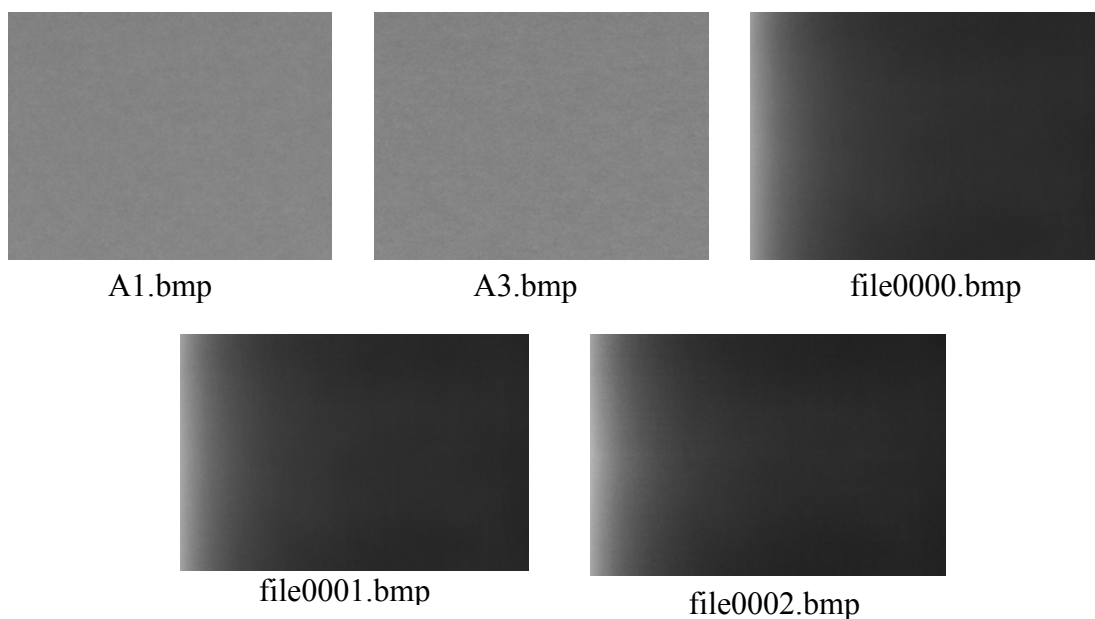


**Figure 1.6** Images used in the study.

## 1.8 Outline of Thesis

This thesis focuses on the comparison of NPS properties of X-ray medical imaging systems. There are 5 chapters; the first chapter provides background of study, problem statement, aim of the study, objective of the study, scope of study, study area and significance of the study. Chapter 2 provides a literature review and theory.

Chapter 3 outlines the steps, techniques and method to be used in this research to achieve the research objectives and outcomes. It also gives a general outline of the steps and methodology used in this research such as data collection, software procedure and others.

Chapter 4 is Results and Analysis. This chapter presents the results of this research and discusses the analysis carried based on the results.

Chapter 5 is Conclusion and Recommendation. It gives the conclusion that has been reached from the study and the completion of this thesis. In this chapter, recommendations are also made based on the findings and analysis.

## References

- Barnes, G. T. (1982). Radiographic mottle: A comprehensive theory. *Medical Physics*, 9(5), 656-667.
- Beutel, J., Yampolsky, M., and Shaw, R. (1993). Comparison of digital Wiener-spectrum calculation methods for screen-film evaluation. *Medical Imaging 1993: Physics of Medical Imaging*. 14 - 19 February 1992. Newport Beach, California: Society of Photo-Optical Instrumentation Engineers, 320-329.
- Broersen, P. M. T. (2005). The uncertainty of measured autocorrelation functions. *2005 IEEE International Workshop on Advanced Methods for Uncertainty Estimation in Measurement, AMUEM 2005*. Niagara Falls, Ontario: IEEE, 90-95.
- Cantell, G. D. (1995). *Measurement of image quality in nuclear medicine and radiology*. Doctor Philosophy, University of Aberdeen, Scotland.
- Cho, H. M., Kim, H. J., Lee, C. L., Nam, S., and Jung, J. Y. (2007). Imaging characteristics of the direct and mobile indirect digital radiographic systems. *2007 IEEE Nuclear Science Symposium and Medical Imaging Conference, NSS-MIC*. 27 October - 3 November 2007. Honolulu, Hawaii: IEEE, 3840-3846.
- Cooley, J. W., and Tukey, J. W. (1965). An algorithm for machine computation of Fourier series. *Mathematics of Computation*, 19, 297-300.
- Cowen, A. R., and Workman, A. (1990). A quantitative investigation of the noise process in digital spot fluorography. In J. Robertson, P. Wankling, K.

- Faulkner and M. Holubinka (Eds.), *Computer in Diagnostic Radiology* (pp. 119-132). York: IPSM.
- Cunningham, I. A. (1999). Image quality and dose. In J. A. Seibert, L. J. Filipow and K. P. Andriole (Eds.), *Practical Digital Imaging and PACS* (pp. 225-258). Madison, WI: Medical Physics Publishing Corporation.
- Cunningham, I. A. (2000). Applied Linear-System Theory. In J. Beutel, H. L. Kundel and R. L. V. Metter (Eds.), *Handbook of Medical Imaging* (Vol. 1, pp. 79-162). Bellingham: SPIE.
- Dainty, J. C., and Shaw, R. (1974). *Image Science*. New York: Academic Press.
- De Belder, M., and De Jerf, J. (1967). The determination of the Wiener spectrum of photographic emulsion layers with digital methods. *Photographic Science and Engineering*, 11, 371-375.
- Dobbins III, J. T., Ergun, D. L., Rutz, L., Hinshaw, D. A., Blume, H., and Clark, D. C. (1995). DQE(f) of four generations of computed radiography acquisition devices. *Medical Physics*, 22(10), 1581-1593.
- Dobbins III, J. T. (2000). Image quality metrics for digital systems. In J. Beutel, H. L. Kundel and R. L. V. Metter (Eds.), *Handbook of Medical Imaging* (Vol. 1, pp. 161-222). Bellingham: SPIE Pubs.
- Dobbins III, J. T., Samei, E., Ranger, N. T., and Chen, Y. (2006). Intercomparison of methods for image quality characterization. II. Noise power spectrum. *Medical Physics*, 33(5), 1466-1475.
- Doerner, E. C. (1962). Wiener spectrum analysis of photographic granularity. *Journal of the Optics Society of America*, 52, 669-672.
- Doi, K. (1966). Scans in Measuring Wiener Spectra for Photographic Granularity. *Japanese Journal of Applied Physics*, 5(12), 1213-1216.

- Doi, K., and Rossmann, K. (1975). Measurements of optical and noise properties of screen film systems in radiography. *Proceedings of the Society of Photo-Optical Instrumentation Engineers*, 56, 45-53.
- Doi, K., Holje, G., Loo, L. N., Chan, H. P., Sandrik, J. M., Jennings, R. J., (1982). *MTFs and Wiener spectra of radiographic screen-film systems*. Rockville, Maryland: U.S. Department of Health and Human Service, Food Drug Administration, Center for Devices and Radiological Health.
- Felleget, P. B. (1953). Concerning photographic grain, signal-to-noise ratio, and information., . *Journal of the Optics Society of America*, 43, 271-281.
- Fisher, M. G. (1982). MTF, noise power spectrum and DQE of radiographic screens. *Photographic Science and Engineering*, 26(1), 32-41.
- Floyd, C.E., Warp, R. J., Dobbins III, J. T., Chotas, H. G., Baydush, A. H., Vargas-Voracek, R., et al. (2001). Imaging characteristics of an amorphous silicon flat-panel detector for digital chest radiography. *Radiology*, 218(3), 683-688.
- Flynn, M. J., and Samei, E. (1999). Experimental comparison of noise and resolution for 2k and 4k storage phosphor radiography systems. *Medical Physics*, 26(8), 1612-1622.
- Funama, Y., Awai, K., Miyazaki, O., Nakayama, Y., Goto, T., Omi, Y., et al. (2006). Improvement of low-contrast detectability in low-dose hepatic multidetector computed tomography using a novel adaptive filter: Evaluation with a computer-simulated liver including tumors. *Investigative Radiology*, 41(1), 1-7
- Goertzen, A. L., Nagarkar, V., Street, R. A., Paulus, M. J., Boone, J. M., and Cherry, S. R. (2004). A comparison of x-ray detectors for mouse CT imaging. *Physics in Medicine and Biology*, 49(23), 5251-5265.

- Granfors, P. R., and Aufrichtig, R. (2000). Performance of a 41x41-cm<sup>2</sup> amorphous silicon flat panel x-ray detector for radiographic imaging applications. *Medical Physics*, 27(6), 1324-1331.
- Hanson, K. M. (1981). Noise and contrast discrimination in computed tomography. *In Radiology of the Skull and Brain, Technical Aspects of Computed Tomography*, 5, 3941-3955.
- Hanson, K. M. (1998). Simplified method of estimating noise-power spectra. In J. T. Dobbins & J. M. Boone (Eds.), *Physics of Medical Imaging* (Vol. 3336, pp. 243-250).
- Harris, F. J. (1978). On the use of windows for harmonic analysis with the discrete Fourier transform. *Proceedings of the IEEE*, 66(1), 51-83.
- Hertich, P. (2005). *Practical Radiography: Principles and applications*. Erlangen: Publics Corporate Publishing.
- Hillen, W., Schiebel, U., and Zaengel, T. (1987). Imaging performance of a digital storage phosphor system. *Medical Physics*, 14(5), 744-751.
- Hoeschen, D., and Mirande, W. (1985). Image quality parameters of screen-film combinations: modulation transfer function and Wiener spectrum. *British journal of radiology. Supplement*, 18, 32-35.
- Hoheisel, M. (2006). Review of medical imaging with emphasis on X-ray detectors. *Nuclear Instruments and Methods in Physics Research, Section A: Accelerators, Spectrometers, Detectors and Associated Equipment*, 563(1), 215-224.
- Holland, R. S. (1979). Fundamentals of radiographic Noise, . In A. G. Haus (Ed.), *The Physics of Medical Imaging: Recoding Systems Measurements and*

*Techniques* (pp. 152-171. ). New York,,: American Assoc. of Physicists in Medicine.

ICRU. (1995). *Medical Imaging-The Assessment of Image quality, ICRU Report 54*, . Bethesda, Maryland ,USA.: International Commission on Radiation Units and Measurements.

Jennings, R. J., Jafroudi, H., Gagne, R. M., Fewell, T. R., Quinn, P. W., Steller Artz, D. E., et al. (1996). Storage phosphor-based digital mammography using a low-dose x-ray system optimized for screen-film mammography. *Medical Imaging 1996: Physics of Medical Imaging*. 11 - 13 February 1996. Newport Beach, California: IEEE, 220-232.

Jessen, K. A. (2004). Balancing image quality and dose in diagnostic radiology. *European Radiology, Supplement*, 14(1), 9-18.

Jiang, H., Chen, W. R., and Liu, H. (2002). Techniques to improve the accuracy and to reduce the variance in noise power spectrum measurement. *IEEE Transactions on Biomedical Engineering*, 49(11), 1270-1278.

Jones, R. C. (1955). New Method of Describing and Measuring the Granularity of Photographic Materials. *J. Opt. Soc. Am.*, 45(10), 799-808.

Kim, J. Y., Park, J. K., Choi, J. Y., Cha, B. Y., Kang, S. S., An, S. H., et al. (2004). Experimental evaluation of a-Se flat-panel X-ray detector for digital radiography. *2004 Nuclear Science Symposium, Medical Imaging Conference, Symposium on Nuclear Power Systems and the 14th International Workshop on Room Temperature Semiconductor X- and Gamma- Ray Detectors*. Rome: IEEE, 4048-4052.

Koedooder, K., Strackee, J., and Venema, H. W. (1986). A new method for microdensitometer slit length correction of radiographic noise power spectra. *Medical Physics*, 13(4), 469-473.

- Lança, L., and Silva, A. (2009). Digital radiography detectors - A technical overview: Part 2. *Radiography*, 15(2), 134-138.
- Lazzari, B., Belli, G., Gori, C., and Rosselli Del Turco, M. (2007). Physical characteristics of five clinical systems for digital mammography. *Medical Physics*, 34(7), 2730-2743.
- Lee, D. L., Cheung, L. K., Palecki, E. F., and Jeromin, L. S. (1996). Discussion on resolution and dynamic range of Se-TFT direct digital radiographic detector. *Medical Imaging 1996: Physics of Medical Imaging*. 11 - 13 February 1996Newport Beach, California: IEEE, 511-522.
- Lissak Giger, M., Doi, K., and Metz, C. E. (1984). Investigation of basic imaging properties in digital radiography. 2. Noise Wiener spectrum. *Medical Physics*, 11(6), 797-805.
- Liu, X., and Shaw, C. C. (2004). a-Si:H/CsI(Tl) flat-panel versus computed radiography for chest imaging applications: Image quality metrics measurement. *Medical Physics*, 31(1), 98-110.
- Maidment, A. D. A., and Yaffe, M. J. (1994). Analysis of the spatial-frequency-dependent DQE of optically coupled digital mammography detectors. *Medical Physics*, 21(6), 721-729.
- Marsh, D. M., and Malone, J. F. (2001). Methods and materials for the measurement of subjective and objective measurements of image quality. *Radiation Protection Dosimetry*, 94(1-2), 37-42.
- Marshall, N. W. (2006). A comparison between objective and subjective image quality measurements for a full field digital mammography system. *Physics in Medicine and Biology*, 51(10), 2441-2463.
- Martin, C. J., Sharp, P. F., and Sutton, D. G. (1999). Measurement of image quality in diagnostic radiology. *Applied Radiation and Isotopes*, 50(1), 21-38.

- Metz, C. E., and Doi, K. (1979). Transfer function analysis of radiographic imaging systems. *Physics in Medicine and Biology*, 24(6), 1079-1106.
- Michitaka, H., and Kunio, S. (2004). An Image Processing Method for Fluoroscopy using a Linear Shadow Detection. *Med Imaging and Inf Sci*, 21, 239-251.
- Monnin, P., Gutierrez, D., Bulling, S., Guntern, D., and Verdun, F. R. (2007). A comparison of the performance of digital mammography systems. *Medical Physics*, 34(3), 906-914.
- Moy, J. P. (1999). Large area X-ray detectors based on amorphous silicon technology. *Thin Solid Films*, 337(1-2), 213-221.
- Nambu, K., and Iseki, H. (2005). A noise reduction method based on a statistical test of high dimensional pixel vectors for dynamic and volumetric images. *Rivista di Neuroradiologia*, 18(1), 21-33.
- Nishikawa, R. M., and Yaffe, M. J. (1985). Signal-to-noise properties of mammographic film-screen systems. *Medical Physics*, 12(1), 32-39.
- Nishiki, M., Shiraishi, K., Sakaguchi, T., and Nambu, K. (2008). Method for reducing noise in X-ray images by averaging pixels based on the normalized difference with the relevant pixel. [10.1007/s12194-008-0028-z]. *Radiological Physics and Technology*, 1(2), 188-195.
- Oppelt, A. E. (2005). *Imaging Systems for Medical Diagnostics: Fundamentals, technical solutions and applications for systems applying ionization radiation, nuclear magnetic resonance and ultrasound*. Erlangen, Germany: Publicis Publishing.
- Park, H.-S., Hee-Joung, K., Hyo-Min, C., Jiyoung, J., and Chang-Lae, L. (2008). *Measurements and evaluation of the image noise power spectrum for computed radiography*. Paper presented at the Nuclear Science Symposium Conference Record, 2008. 19-25 Oct. 2008. NSS '08: IEEE, 4378-4383.

- Porat, B. (1994). *Digital Processing of Random Signals*. Englewood Cliffs, NJ.: Prentice-Hall.
- Press, W. H., Flannery, B. P., Teukolsky, S. A., and Vetterling, W. T. (1998). *Numerical recipes in C*. Cambridge: Cambridge University Press.
- Rossmann, K. (1962). Modulation Transfer Function of Radiographic Systems Using Fluorescent Screens. *J. Opt. Soc. Am.*, 52(7), 774-775.
- Rossmann, K. (1963). Image-forming quality of radiographic screen-film systems: the line spread-function. *The American journal of roentgenology, radium therapy, and nuclear medicine*, 90, 178-183.
- Saito, N., Kudo, K., Sasaki, T., Uesugi, M., Koshino, K., Miyamoto, M., et al. (2008). Realization of reliable cerebral-blood-flow maps from low-dose CT perfusion images by statistical noise reduction using nonlinear diffusion filtering. *Radiological Physics and Technology*, 1(1), 62-74.
- Samei, E. (2003). Image quality in two phosphor-based flat panel digital radiographic detectors. *Medical Physics*, 30(7), 1747-1757.
- Samei, E., and Flynn, M. J. (2003). An experimental comparison of detector performance for direct and indirect digital radiography systems. *Medical Physics*, 30(4), 608-622.
- Samei, E., Ranger, N. T., Mackenzie, A., Honey, I. D., Dobbins III, J. T., and Ravin, C. E. (2009). Effective DQE (eDQE) and speed of digital radiographic systems: An experimental methodology. *Medical Physics*, 36(8), 3806-3817.
- Sandrik, J. M., and Wagner, R. F. (1981). Radiographic screen-film noise power spectrum: variation with microdensitometer slit length. *Applied Optics*, 20(16), 2795-2798.

- Sandrik, J. M., and Wagner, R. F. (1982). Absolute measures of physical quality: Measurement and application to radiographic magnification. *Medical Physics*, 9(4), 540-549.
- Sandrik, J. M., Wagner, R. F., and Hanson, K. M. (1982). Radiographic screen-film noise power spectrum: Calibration and intercomparison. *Applied Optics*, 21(19), 3597-3601.
- Schade, O. H. (1952). Image gradation, graininess, and sharpness in television and motion picture systems: part II—the grain structure of motion picture images: an analysis of deviations and fluctuations of the sample number. *J. Soc. Motion Picture and Television Engineers*, 58, 181–222.
- Schade, O. H. (1953). Image gradation, graininess, and sharpness in television and motion picture systems: part III—the grain structure of motion picture images: an analysis of deviations and fluctuations of the sample number. *J. Soc. Motion Picture and Television Engineers*, 61, 67-164.
- Selwyn, E. W. H. (1935). A theory of graininess. *Photographic Journal*, 75, 571-580.
- Sidentops, H. (1937). Concerning granularity, resolution and enlargement of photographic negatives. *Phsik Ziet*, 38, 454-459.
- Smith, A. (2003). Fundamentals of digital mammography: physics, technology and practical considerations. *Radiology Management*, 25(5), 18-24.
- Sturm, R. E., and Morgan, R. H. (1949). Screen intensification systems and their limitations. *The American journal of roentgenology, radium therapy, and nuclear medicine*, 62(5), 617-634.
- Suryanarayanan, S., Karellas, A., and Vedantham, S. (2004). Physical characteristics of a full-field digital mammography system. *Nuclear Instruments and Methods in Physics Research, Section A: Accelerators, Spectrometers, Detectors and Associated Equipment*, 533(3), 560-570.

- Van Metter, R., and Dickerson, R. (1994). Objective performance characteristics of a new asymmetric screen-film system. *Medical Physics*, 21(9), 1483-1490.
- Vuylsteke, P., and Dewaele, P. (1995). United States Patent No. 5461655. B. E. Morstel & B. E. Berhcem.
- Wagner, R. F. (1977). Fast Fourier digital quantum mottle analysis with application to rare earth intensifying screen systems. *Medical Physics*, 4, 157-162.
- Wan Hassan, W. M. S. (1998). *Measurement of Modulation Transfer Function and Wiener Spectrum of Diagnostic X-Ray Screen-Film Systems in a Hospital Setting*. Doctor Philosophy, University of Aberdeen, Scotland.
- Wan Hassan, W. M. S. (2001). Measurement of Wiener spectrum of radiographic screen-film systems. *Jurnal Teknologi*, 34(C), 35-42.
- Welch, P. (1967). The use of fast Fourier transform for the estimation of power spectra: A method based on time averaging over short, modified periodograms. *Audio and Electroacoustics, IEEE Transactions on*, 15(2), 70-73.
- Williams, M. B., Mangiafico, P. A., and Simoni, P. U. (1999). Noise power spectra of images from digital mammography detectors. *Medical Physics*, 26(7), 1279-1293.
- Yamada, S., and Murase, K. (2005). Effectiveness of flexible noise control image processing for digital portal images using computed radiography. *British Journal of Radiology*, 78(930), 519-527.
- Zhang, D., Liu, H., and Wu, X. (2008). DQE analysis on a dual detector phase x-ray imaging system. *Physics in Medicine and Biology*, 53(18), 5165-5176.

Zhang, D., Rong, J., Chen, W. R., Gao, F., Xu, K., Wu, X., et al. (2007). Impact of additive noise on system performance of a digital X-ray imaging system. *IEEE Transactions on Biomedical Engineering*, 54(1), 69-73.